2014 International Conference on Unmanned Aircraft Systems (ICUAS)
May 27-30, 2014. Orlando, FL, USA

Rigid vs. Flapping: The Effects of Kinematic Formulations in Force Determination of a Free Flying Flapping Wing Micro Air Vehicle

J. V. Caetano*†, M. B. Weehuizen*, C. C. de Visser*, G.C.H.E. de Croon*, C. de Wagter*, B. Remes* and M. Mulder*
*Section of Control and Simulation, Faculty of Aerospace Engineering, Delft University of Technology, Delft, The Netherlands
†Air Force Research Laboratory, Portuguese Air Force Academy, Sintra, Portugal
Corresponding author: j.v.caetano@tudelft.nl; DelFly research contact: microuav@gmail.com

***Abstract*—Several studies have focused on deriving kinematic formulations of simulated flapping wing micro air vehicles (FWMAV). However, very few used real-life flight data and none have compared the predicted aerodynamic forces and moments across different kinematic formulation principles. Hence, the present study compares and assesses the quality of simple equations of motion against complex multi-body formulations using real flight data. In particular, the position and attitude of an autonomous flying FWMAV was logged by an external high resolution visual tracking system. States were reconstructed using flight path reconstruction techniques and were used as inputs for the determination of the aerodynamic forces and moments that acted on the FWMAV. Two kinematic models of a 4 wing FWMAV were derived and used to compute the aerodynamic forces and moments: 1) simple Newton-Euler formulation of rigid aircraft equations of motion; 2) complex 5 body kinematic model using D'Alembert's principle. The results are presented for trimmed flight, as well as for system identification maneuvers characterized by doublet inputs on the rudder and elevator. These results show the difference between both formulations and indicate that rigid body kinematic forms can be used for FWMAV aerodynamic system identification, with the advantageous use in control design of iterative versions of ornithopters, showing an average correlation of 0.98 (out of 1) with more complex formulations. Multi-body kinematics, on the other hand, despite more time-expensive to derive, capture more contributions of the different FWMAV structures as well as the internal forces and moments (like driving motor torque), thus being more suitable for simulation and robust control of complex ornithopters.**

I. Introduction

Research in Flapping Wing Micro Air Vehicles (FWMAV) has recently lead to many new developments and applications of FWMAVs. Aerovironment's Nano-Hummingbird [1], Harvard's RoboBee [2], [3], Carnegie Mellon's [4] and UCBerkeley's FWMAV [5] and TU Delft's DelFlys [6], [7] gather at the top of the list of most advanced FWMAV. While the first 3 platforms are tailless designs, for which research focuses on in-flight controllability and autonomy, UCBerkeley's FWMAV and the DelFlys' tailed designs makes them good platforms for applying higher level implementations, such as flight-test driven system identification [8] and autonomous sense-and-avoid [9], [10].

However, there is still a considerable knowledge gap in flapping wing aerodynamic force generating mechanisms, as well as lack of phenomenological models that could be used for on-board nonlinear model-based control strategies. In this regard, the description of flapping wing kinematics would be advantageous for FWMAV aerodynamic model identification, which in turn is essential for flight control design and simulation.

There are numerous mathematical formulations that describe the multi-body relations in a FWMAV with a multitude of studies demonstrating the use of different principles in deriving the equations of motion. Some authors focused on devising complex equations of motion using Newton-Euler formulation [11], Lagrange's energy-based methods [12], [13], D'Alembert's virtual work principle for dynamic systems [14], [15] and Kane's equations [16], or, instead, have used advanced computational aeroelastic techniques to assess the effects of structure flexibility, as well as the dynamic stability of a two-winged FWMAV [17], [18]. Others [19], [20], on the other hand, have used simple aircraft equations of motion with restricted degrees of freedom to simulate the behavior of a bird-like FWMAV and demonstrated method stability, as well as good dynamic results.

All the previous studies were driven by the need to understand and predict the dynamics of FWMAV in simulated environments and only Grauer et al. [12], [13] were able to use a kinematic model and determine the aerodynamic forces acting on a free flying FWMAV for system identification purposes. Nevertheless, none of these studies compared the actual forces and moments computed from flight data using different formulations of the kinematic model.

Complex kinematic formulations can be tortuous to derive and are not practical for iterative system development, as new formulations have to be derived for each change in the FWMAV's design. Furthermore, the ease of determining aerodynamic forces and moments from rigid-body kinematic models would facilitate system identification techniques and the derivation of phenomenological aerodynamic models that could more easily be used for on-board flight control strate-

978-1-4799-2376-2/14/$31.00 ©2014 IEEE

gies and simulations. Moreover, simple formulations would also simplify the study of new FWMAV designs, avoiding the need for new complex formulations and thus allowing a fast initial assessment of the results of design changes.

Hence, the present study focuses on comparing simple general aircraft equations of motion with a more complex multi-body formulation. In particular, this paper presents a quantitative comparison of the forces and moments calculated from flight data using 1) the standard Newton-Euler formulation for rigid aircraft dynamics, and 2) the D'Alembert's principle applied to rigid bodies. To enable this comparison, the position and attitude of the Delfly II FWMAV was recorded using a high resolution visual tracking system during a series of auto-pilot controlled flights. Flight path reconstruction techniques are then applied to the raw tracking system data to calculate the FWMAV states (Section II). Subsequently, the kinematic formulations are derived (Section III) and the results are quantitatively compared (Section IV). The study concludes with an analysis of the applicability of these methods to other FWMAV (Section V).

II. Approach and Methodology

A FWMAV was flown automatically in a flight chamber equipped with a high resolution visual tracking system. Then, flight path reconstruction techniques were used to determine the states that were used as variables in two different kinematic formulations. For better understanding, the present section describes the FWMAV, the experimental techniques and explains the flight path reconstruction methodology.

A. DelFly II Flapping Wing Micro Aerial Vehicle

The DelFly II is a FWMAV developed at Delft University of Technology with 4 wings in 'X' configuration and an inverted 'T' tail (Figures 1 and 2). Its wings are made with Mylar foil and very thin carbon rods and have a closed wing dihedral of 13°. The wing configuration minimizes the flapping-induced oscillations in the body due to the opposite movement of the upper and lower wings, that rotate with symmetric angular velocities and accelerations around $\overrightarrow{x_b}$, as seen in Figure 2.

The ornithopter's tail is made of thin Styrofoam for rapid construction, robustness and visual referencing in flight. It introduces static stability on the platform and can be used for attitude control through its elevator and rudder. It also simplifies the wing design and control strategies by decoupling the lateral control from the wings, thus allowing it to have 2 degrees of freedom (active rotation around $\overrightarrow{x_b}$ and passive rotation around the leading edge spar) with only 1 control input on the motor.

The FWMAV can be configured with different controllers and flown manually through a radio control receiver or autonomously by the setup of a custom-made sense-and-avoid stereo vision payload [10]. For the current test cases, it was configured with an autopilot that was able to maintain a trimmed flight regime, assuring an almost constant pitch angle, vehicle height and velocity throughout its flight [6].

B. Experimental Techniques

An external visual tracking system was used to capture the position of the FWMAV in free flight, in 3D space at a frequency of 200Hz using 8 reflective markers[1]. The markers were placed at the nose, wing trailing edge (on fuselage/body), wings (at the stiffeners' intersection with the leading edge spar), horizontal and vertical stabilizers, as well as on the elevator and rudder, as indicated in Figure 1.

The FWMAV was flown automatically at different trimmed flight attitudes and velocities, while several combinations of input commands where given to the elevator, rudder and flapping motor - the input signals varied from simple step inputs to more sophisticated ones, like multi-step 2-1-1 [21], which induced oscillations on the FWMAV's states around a trimmed flight condition. The inputs were commanded at different frequencies, lasting from $\frac{1}{3}$ seconds to $\frac{4}{3}$ seconds, which excited the platform's dynamic modes. [2]

Fig. 1. The DelFly FWMAV configuration and reflective markers' positions.

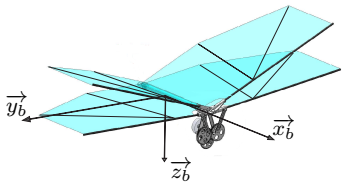

Fig. 2. Wing configuration and Body frame axis ($\overrightarrow{x_b}$, $\overrightarrow{y_b}$, $\overrightarrow{z_b}$)

C. Flight Path Reconstruction

Before each flight the center of gravity (CG) was measured by determining the equilibrium point around a very thin edge and measured with a calliper. The inertia along the principal axis was measured by a moment of inertia unit [3].

The recorded data were processed using flight path reconstruction techniques [22]. After the assessment of the information precision [22], a direct cosine matrix was used to determine the attitude angles by comparing the entries with a 3-2-1 rotation matrix (eq. 2 in [8]) from the visual tracking system (here considered as Inertial) reference frame to the FWMAV Body frame indicated on Figure 3.

Given the fact that only position and attitude can be measured directly, numerical differentiation techniques must be used to determine the body velocities and accelerations. Numerical differentiation of discrete signals can amplify the measurement noise by a factor equal to the sampling

[1]All flight tests in this paper were conducted at the U.S. Air Force Research Laboratory Micro Air Vehicles Integration and Application Institute [21]

[2]For better understanding of the experimental methods, videos were made available at http://www.delfly.nl/icuas2014.html

[3]Inertia Dynamics S.N. MOI-005-004 Moment of Inertia Measurement Instrument, http://www.idicb.com/moimeas.asp

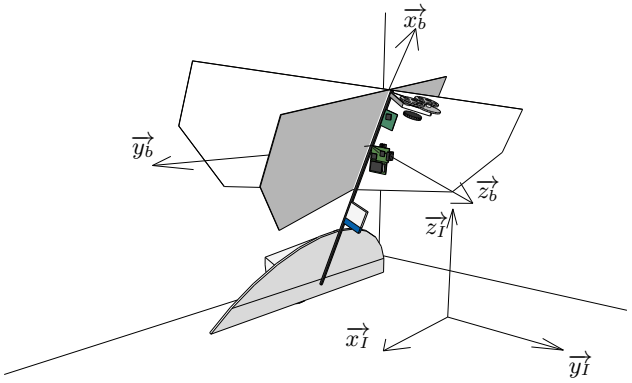

Fig. 3. Inertial ($\overrightarrow{x_I}$, $\overrightarrow{y_I}$,$\overrightarrow{z_I}$) and Body ($\overrightarrow{x_b}$,$\overrightarrow{y_b}$,$\overrightarrow{z_b}$) reference frames.

frequency. A three-point central difference method was used for calculating the velocities and accelerations, which reduces the noise amplification by a factor of 2 when compared with the 2 point finite difference. A possible workaround would be to lower the recording frequency or use 2 or 3 point average position before differentiation. However, this method would smooth the data and reduce the state's information within the flap cycle.

To compensate for the added noise effect, which is more significant at frequencies that are several times the flapping frequency, a Chebyshev type II low-pass filter was used, with -80dB attenuation and 40Hz cut-off frequency. This filter retains the more energetic contributions, which are located at the flapping frequency and the following 2 harmonics.

The states and input commands that were reconstructed are presented in Table I. All states were calculated with respect to the DelFly's CG and were used for the calculation of the external forces and moments from the kinematic formulations that are presented in the following section.

III. Kinematic Formulations

Within a given CG interval, the DelFly is an inherently stable platform in open-loop. Moreover, the control strategies are also relatively simple, as these have to be devised for flap cycle averaged forces and moments since the wings are not used for direct attitude control, being only used for lift and thrust generation.

Two kinematic formulations were used to compute the acting forces and moments during the DelFly's free flight. These have different underlying approaches: the first formulation is a Newton-Euler method that was used for the derivation of the equations of motion of a rigid non-flapping body, also typically known as the general aircraft equations of motion; the second uses d'Alembert's the virtual work principle applied to rigid bodies to determine the kinematics of a flapping platform, using the DelFly's physical properties.

A. Rigid Body Kinematic Model

The Newton-Euler derivation of the general aircraft equations of motion is used for the rigid body kinematic formulation and is presented in Eq. 1. The (X, Y, Z) and (L, M, N) are the acting aerodynamic forces and moments, respectively, in the Body axes ($\overrightarrow{x_b}$, $\overrightarrow{y_b}$, $\overrightarrow{z_b}$) [23]:

$$
\begin{aligned}
X &= m(g\sin\theta + \dot{u} + qw - rv)\\
Y &= m(-g\sin\phi\cos\theta + \dot{v} + ru - pw)\\
Z &= m(-g\cos\phi\cos\theta + \dot{w} + pv - qu)\\
L &= I_x\dot{p} - I_{xz}(\dot{r} + pq) + (I_z - I_y)qr\\
M &= I_y\dot{q} + (I_x - Iz)rp + I_{xz}(p^2 - r^2)\\
N &= I_z\dot{r} - I_{xz}\dot{p} + (I_y - I_x)pq + I_{xz}rq\\
\dot{\psi} &= (q\sin\phi + r\cos\phi)/cos\theta\\
\dot{\theta} &= q\cos\theta - r\sin\theta\\
\dot{\phi} &= p + (q\ sin\phi + r\cos\phi)tan\theta
\end{aligned}
\tag{1}
$$

Six assumptions were taken in this rigid body kinematic formulation: a) non-flapping rigid body; b) constant mass c) no inertia changes due to flapping or bending; d) symmetric platform; e) stationary atmosphere; f) flat Earth.

1) Applicability Aspects: One may argue about the applicability of the general aircraft equations of motion to FWMAVs as these do not account for any moving parts and consider the inertia as being constant between two consecutive time-steps. Moreover, the non-flapping applicability region depends not only on the wing-generated forces and moments' evolution over the flap cycle, but also on the wing mass and inertia to body mass and inertia ratio, respectively. However, the rigid body formulation benefits from being easily devised for non-exotic aircraft configurations while still taking into consideration the accelerations and Coriolis couplings of rigid body dynamics. Furthermore, the DelFly's wing configuration minimizes the inertia distribution changes over a flap cycle, as the lower wing rotation counteracts the upper wing's to a great extent. Another facto justifying the assumption is that the FWMAV does not require the full discretization of its flapping kinematics for onboard control.

Except for the tail and its electronics, the DelFly is manually built and configured, which makes it not perfectly symmetric around the x_bz_b plane. However, the symmetry assumption is justified by the fact that the moment of inertia around the body $\overrightarrow{x_b}$ is 2 orders of magnitude smaller than the moments of inertia around the other principal axis, making the coupled I_{xy}, I_{yz} negligible, here assumed to be zero.

The aerodynamic forces are significantly affected by a non-stationary atmosphere. Since we have no measurements of the air flow around the FWMAV, they are assumed to not be present for estimation. Furthermore, the flight chamber that was used has a volume of $(22\times17\times10)\text{m}^3$, is fully closed and does not contain air outlets. Moreover, the FWMAV was flown far from the wall, where the flapping induced flow could have effects over the FWMAV's perceived free stream. Some of the maneuvers induced, however, transient aerodynamic effects that affect the flow distribution over the FWMAV, e.g., step reductions in the flapping motor command. For the sake of comparison, these test flights were

TABLE I
STATES AND INPUT COMMANDS RECONSTRUCTED FROM FLIGHT DATA.

Quaternions	Euler Angles	Euler Angle Rates	Velocities	Accelerations	Angular Body Rates	Angular Body Accelerations	Inputs	Flapping
e_0	ϕ	$\dot{\phi}$	u	$\dot{u}$	p	$\dot{p}$	ζ	δ_f(flap freq.)
e_1	θ	$\dot{\theta}$	v	$\dot{v}$	q	$\dot{q}$	$\dot{\zeta}$	δ_e(elevator)
e_2								
e_3	ψ	$\dot{\psi}$	w	$\dot{w}$	r	$\dot{r}$	$\ddot{\zeta}$	δ_r(rudder)

left out, as they would affect the flow distribution regardless of the described kinematic model.

The last 3 equations of the kinematic formulation in Eq. 1 are not well defined for pitch angles close to 90°, i.e., when the θ is above 80°, a slight change in yaw will induce a fast variation in ψ, resulting in bad information on $\dot{\psi}$ and consequently bad r calculation. The same happens to the roll angle, as a rotation around $\overrightarrow{z_b}$ affects the heading angle ψ, which in turn results in a rolling miss-information on the Euler angles. Moreover, the DelFly is able to fly backwards, in inverted flight for short periods of time in transitioning maneuvers. This way, Body angular velocities and accelerations cannot be determined from the Euler angles, i.e., if the DelFly performs a looping, its pitch rate q is always positive while the $\dot{\theta}$ is negative during inverted flight. On top of this, the singularity makes it impossible to calculate the Euler angles, and hence, the rotational rates p, q and r around 90°.

The DelFly can enter such singularity conditions for certain elevator pitch-up maneuvers. Thus, to prevent p, q, r from feeding wrong information into the force and moments equations, new attitude angles were devised, that replaced the Euler angles with ϕ_r, θ_p, ψ_y for the roll, pitch and yaw angles, respectively. The method assumes that for pitch angles between in [82°;98°] the roll and yaw are considered constant and the θ_p becomes bigger than 90° if the FWMAV is flying inverted.

B. Flapping Wing Kinematics

1) The DelFly model: The DelFly is modeled as combination of 5 rigid bodies. First, there is the main body (B) consisting of the carbon rod and the hardware attached to the rod. Also the vertical and horizontal tails are part of the main body. The other bodies consist of the four wings, referenced as W1, W2, W3 and W4, which are assumed to rotate around $\overrightarrow{x_b}$, as indicated in Figure 4.

a) Body Reference Frame (B): The Body fixed reference frame is attached to the main body B, with the origin on its CG. The main body is aligned with the $\overrightarrow{x_b}$ axis. The $\overrightarrow{y_b}$ axis is pointing out of the right side of the DelFly. The $\overrightarrow{z_b}$ is pointing downwards, perpendicular to the $x_b y_b$ plane. The reference frame is also showed in the Figure 4.

b) Wing Frame (W): A separate reference frame was used for each wing, with its origin at the hinge point and the $x_w y_w$ plane coincident with the wing surface. The frames are assumed to rotate with the wing around $\overrightarrow{x_b}$.

c) Flap angle ζ: When the two wings at one side of the DelFly are 'closed', the wings make dihedral angle ζ_0 with an horizontal line parallel to the $\overrightarrow{y_b}$ axis and running through the hinge point. The flapping angle ζ is specified from ζ_0 to the wing and is the same for all wings, as shown in Figure 4.

In order to specify the motion of the center of mass of all wing bodies in the Body frame (B), a position vector $\boldsymbol{\rho}_{h,b}$ is defined as the position of the hinge point with respect to the center of mass of the main body. A second vector, in the Body frame, is specified from the hinge point to the center of mass of the wings $\boldsymbol{\rho}_{w,h}$. These position vectors are shown in Figure 5.

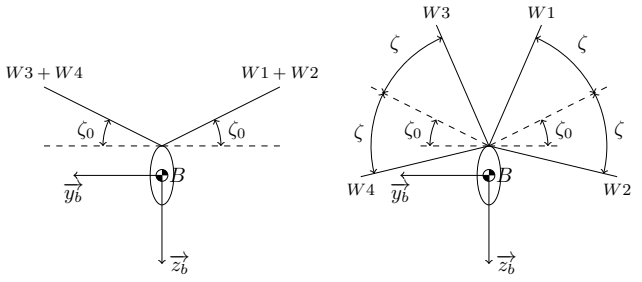

(a) Model with wings closed (b) Model with wings open at an angle ζ

Fig. 4. Simplified Model of the DelFly, with the Body reference frame B and Wing frames, W1 to W4. The angles ζ_0 and ζ form the dihedral and wing aperture angle, respectively.

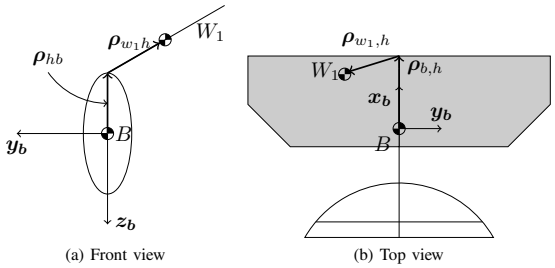

(a) Front view (b) Top view

Fig. 5. DelFly model with $\boldsymbol{\rho}_{h,b}$ and $\boldsymbol{\rho}_{w,h}$ representation.

d) From Body Frame to Wing Frames: The transformation from the Body frame to the Wing frames consisted of only one rotation around the $\overrightarrow{x_b}$ axis and are be defined as:

$$\mathcal{R}_{w1,b}=\begin{bmatrix}1 & 0 & 0\\ 0 & cos(\zeta_0+\zeta) & sin(\zeta_0+\zeta)\\ 0 & -sin(\zeta_0+\zeta) & cos(\zeta_0+\zeta)\end{bmatrix}$$
$$\mathcal{R}_{w2,b}=\begin{bmatrix}1 & 0 & 0\\ 0 & cos(\zeta_0-\zeta) & sin(\zeta_0-\zeta)\\ 0 & -sin(\zeta_0-\zeta) & cos(\zeta_0-\zeta)\end{bmatrix}$$
$$\mathcal{R}_{w3,b}=\begin{bmatrix}1 & 0 & 0\\ 0 & cos(-\zeta_0-\zeta) & sin(-\zeta_0-\zeta)\\ 0 & -sin(-\zeta_0-\zeta) & cos(-\zeta_0-\zeta)\end{bmatrix} \quad (2)$$
$$\mathcal{R}_{w4,b}=\begin{bmatrix}1 & 0 & 0\\ 0 & cos(-\zeta_0+\zeta) & sin(-\zeta_0+\zeta)\\ 0 & -sin(-\zeta_0+\zeta) & cos(-\zeta_0+\zeta)\end{bmatrix}$$

e) From Inertia frame to Body frame: The transformation from the Inertia frame to the Body frame is done using the Quaternions. There are two advantages of this formulation: a) the gain in computational efficiency when compared with a formulation based on Euler angles, making it more suitable for onboard model based control applications; b) the ability to overcome the 'Euler singularity', at pitch angle θ=90°, as well as avoiding bad rotational information for very high pitch angles. The rotation matrix becomes [24]:

$$\mathcal{R}_{b,I}=\begin{bmatrix}e_1^2+e_0^2-e_2^2-e_3^2 & 2(e_1e_2+e_3e_0) & 2(e_1e_3-e_2e_0)\\ 2(e_1e_2-e_3e_0) & -e_2^2-e_0^2+e_1^2+e_3^2 & 2(e_2e_3+e_1e_0)\\ 2(e_1e_3+e_2e_0) & 2(e_2e_3-e_1e_0) & -e_3^2-e_0^2+e_1^2+e_2^2\end{bmatrix} \quad (3)$$

The angular velocities in the body frame can now be determined using:

$$\begin{bmatrix}0\\ p\\ q\\ r\end{bmatrix}=2\begin{bmatrix}e_0 & e_1 & e_2 & e_3\\ -e_1 & e_0 & e_3 & -e_2\\ -e_2 & -e_3 & e_0 & e_1\\ -e_3 & e_2 & -e_1 & 0\end{bmatrix}\begin{bmatrix}\dot{e_0}\\ \dot{e_1}\\ \dot{e_2}\\ \dot{e_3}\end{bmatrix} \quad (4)$$

2) Generalized coordinates and Quasi-velocities: The main body B has 6 Degrees Of Freedom (DOF) in Inertial space; the four wing bodies (W_1 to W_4) are attached to the main body and it is assumed that they can only rotate around one axis, hence they have only 1 DOF. Since they are all driven by the same motor and the motion of all wings is coupled, this motion can be defined with only one generalized coordinate ζ.

There are 8 generalized coordinates: the inertial position of the main body (x,y,z), the Quaternion terms (e_0, e_1, e_2, e_3) and the flap angle (ζ).

$$\boldsymbol{q}_j = [x, y, z, e_0, e_1, e_2, e_3, \zeta] \quad (5)$$

There are also 8 generalized velocities, which correspond to the time derivatives of $\boldsymbol{q}_j$. Nevertheless, there are only seven quasi-velocities thanks to 1 non-holonomic [25] constraint in the generalized coordinates, caused by the Quaternion definition. Hence, the quasi-velocities are formed by the linear velocities *(u,v,w)*, the angular velocities *(p,q,r)* and the time derivative of the flapping angle ($\dot{\zeta}$), as follows:

$$\boldsymbol{u}_j = [u, v, w, p, q, r, \dot{\zeta}] \quad (6)$$

3) Velocities: The translational velocities for each rigid body written in the body frame are:

$$\begin{aligned}\boldsymbol{v}_1 &= u\boldsymbol{b}_x + v\boldsymbol{b}_y + w\boldsymbol{b}_z\\ \boldsymbol{v}_2 &= \boldsymbol{v}_1 + \boldsymbol{\omega}_1 \times \boldsymbol{\rho}_{h,b} + \boldsymbol{\omega}_2 \times \boldsymbol{\rho}_{b_{w1,h}}\\ \boldsymbol{v}_3 &= \boldsymbol{v}_1 + \boldsymbol{\omega}_1 \times \boldsymbol{\rho}_{h,b} + \boldsymbol{\omega}_3 \times \boldsymbol{\rho}_{b_{w2,h}}\\ \boldsymbol{v}_4 &= \boldsymbol{v}_1 + \boldsymbol{\omega}_1 \times \boldsymbol{\rho}_{h,b} + \boldsymbol{\omega}_4 \times \boldsymbol{\rho}_{b_{w3,h}}\\ \boldsymbol{v}_5 &= \boldsymbol{v}_1 + \boldsymbol{\omega}_1 \times \boldsymbol{\rho}_{h,b} + \boldsymbol{\omega}_5 \times \boldsymbol{\rho}_{b_{w4,h}}\end{aligned} \quad (7)$$

and the angular velocities are defined as:

$$\begin{aligned}\boldsymbol{\omega}_1 &= p\boldsymbol{b}_x + q\boldsymbol{b}_y + r\boldsymbol{b}_z\\ \boldsymbol{\omega}_2 &= (p+\dot{\zeta})\boldsymbol{b}_x + q\boldsymbol{b}_y + r\boldsymbol{b}_z\\ \boldsymbol{\omega}_3 &= (p-\dot{\zeta})\boldsymbol{b}_x + q\boldsymbol{b}_y + r\boldsymbol{b}_z\\ \boldsymbol{\omega}_4 &= (p-\dot{\zeta})\boldsymbol{b}_x + q\boldsymbol{b}_y + r\boldsymbol{b}_z\\ \boldsymbol{\omega}_5 &= (p+\dot{\zeta})\boldsymbol{b}_x + q\boldsymbol{b}_y + r\boldsymbol{b}_z\end{aligned} \quad (8)$$

4) Accelerations: The velocity vectors $\boldsymbol{v}_i$ are defined in the rotating Body frame. Hence, the acceleration of the main body becomes:

$$\dot{\boldsymbol{v}}_1 = \frac{\partial \boldsymbol{v}_1}{\partial t} + \boldsymbol{\omega}_1 \times \boldsymbol{v}_1 \quad (9)$$

where, $\frac{\partial \boldsymbol{v}_1}{\partial t}$ is the change in speed observed from the rotating B frame defined in Eq. (10). The second term is the acceleration caused by the rotation of the reference frame.

$$\frac{\partial \boldsymbol{v}_1}{\partial t} = \dot{u}\boldsymbol{b}_x + \dot{v}\boldsymbol{b}_y + \dot{w}\boldsymbol{b}_z \quad (10)$$

The translational accelerations of wing rigid bodies are then:

$$\dot{\boldsymbol{v}}_i = \frac{\partial \boldsymbol{v}_i}{\partial t} + \boldsymbol{\omega}_1 \times \boldsymbol{v}_i \quad \text{with} \quad i = 2, 3, 4, 5 \quad (11)$$

The angular accelerations in the Body frame are obtained using Eq. 12:

$$\begin{aligned}\dot{\boldsymbol{\omega}}_1 &= \frac{\partial \boldsymbol{\omega}_1}{\partial t} = \dot{p}\boldsymbol{b}_x + \dot{q}\boldsymbol{b}_y + \dot{r}\boldsymbol{b}_z\\ \dot{\boldsymbol{\omega}}_2 &= \frac{\partial \boldsymbol{\omega}_2}{\partial t} + \boldsymbol{\omega}_1 \times \boldsymbol{\omega}_2\\ \dot{\boldsymbol{\omega}}_3 &= \frac{\partial \boldsymbol{\omega}_3}{\partial t} + \boldsymbol{\omega}_1 \times \boldsymbol{\omega}_3\\ \dot{\boldsymbol{\omega}}_4 &= \frac{\partial \boldsymbol{\omega}_4}{\partial t} + \boldsymbol{\omega}_1 \times \boldsymbol{\omega}_4\\ \dot{\boldsymbol{\omega}}_5 &= \frac{\partial \boldsymbol{\omega}_5}{\partial t} + \boldsymbol{\omega}_1 \times \boldsymbol{\omega}_5\end{aligned} \quad (12)$$

5) Mass, CG Position and Inertia Moments: The CG position and the mass moment of inertia for the complete DelFly that was used are know [21].

TABLE II
MASS OF WING COMPONENTS

	Mass (g)
Leading Edge Rod	0.168
Stiffeners (2x)	0.01
Mylar Foil	0.110
Complete Wing	0.298

TABLE III
MOMENTS OF INERTIA OF THE BODY AND WINGS

Moment	Body	Wing
I_x	$9.64167E^{-7}$	$4.4354E^{-07}$
I_y	$9.64167E^{-5}$	$1.7438E^{-07}$
I_z	$7.85967E^{-5}$	$8.7337E^{-07}$

a) Wing: The position of the center of mass of each wing in the Body frame is necessary to define their relative motion. First the position of the center of mass of a wing is defined on its own Wing frame as $\boldsymbol{\rho}_{w,h}$ (Figure 5). This position vector can then be transformed to the Body frame using the transpose of the transformation matrices found in Eq. 2, resulting in:

$$\boldsymbol{\rho}_{b_{wi,h}} = \mathcal{R}_{b,wi}\boldsymbol{\rho}_{wi,h} \quad \text{with} \quad i = 1,2,3,4 \tag{13}$$

The position of the center of mass of the wings with respect to the center of mass of the main body $\boldsymbol{\rho}_{w,b}$ is calculated by adding $\boldsymbol{\rho}_{b_{wi,h}}$ to $\boldsymbol{\rho}_{h,b}$, which is the position of the hinge point with respect to the center of mass of the main body (B).

The CG position and inertia moments of the wings were calculated analytically, using the mass of each wing component: leading edge rod, stiffeners and Mylar foil. The CG position and wing layout are shown in Figure 6. The body and wings moments of inertia are presented in Tables II and III.

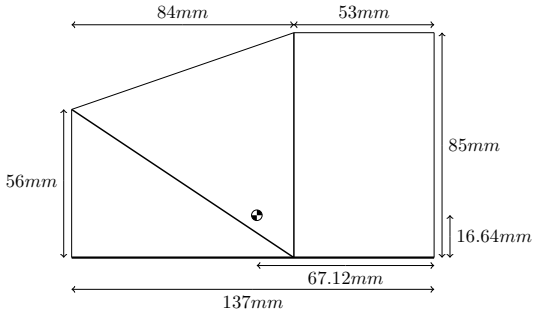

Fig. 6. DelFly wing schematic.

Only the principal moments of inertia of the wing were considered since the crossed terms are very small, forming I_w:

$$I_w = \begin{bmatrix} I_{x,w} & 0 & 0 \\ 0 & I_{y,w} & 0 \\ 0 & 0 & I_{z,w} \end{bmatrix} \tag{14}$$

The inertia matrix can be transformed to the Body frame using the inverse of the transformation matrices of Eq. 2 in:

$$I_w^b = \mathcal{R}_{b,w} I_w \mathcal{R}_{b,w}^T \tag{15}$$

6) Generalized Forces: Let Q_j be the generalized forces related to each quasi-velocity u_j which are defined using the virtual work principle:

$$Q_j = \sum_{i=1}^{n} (\boldsymbol{F_i}\boldsymbol{\gamma_{ij}} + \boldsymbol{M_i}\boldsymbol{\beta_{ij}}) \tag{16}$$

The forces Q_1, Q_2 and Q_3 are the resultant forces along the axes of the Body frame, which include gravity and aerodynamic forces.

The weight vector is expressed in the Body frame using $\mathcal{R}_{b,I}$:

$$\boldsymbol{g_b} = \mathcal{R}_{b,I} \begin{bmatrix} 0 \\ 0 \\ g \end{bmatrix} \tag{17}$$

Hence, the first three generalized forces become:

$$\begin{bmatrix} Q_1 \\ Q_2 \\ Q_3 \end{bmatrix} = \begin{bmatrix} X \\ Y \\ Z \end{bmatrix} + (m_1+m_2+m_3+m_4+m_5)\mathcal{R}_{b,v} \begin{bmatrix} 0 \\ 0 \\ g \end{bmatrix} \tag{18}$$

The following generalized forces (Q_4, Q_5 and Q_6) are the moments in the Body frame, which also include gravity ($\boldsymbol{M_g}$) and aerodynamic (L, M, N) terms:

$$\begin{aligned} \boldsymbol{M_g} = \boldsymbol{\rho_{w_1,b}} \times (m_2\boldsymbol{g_b}) + \boldsymbol{\rho_{w_2,b}} \times (m_3\boldsymbol{g_b}) + \\ + \boldsymbol{\rho_{w_3,b}} \times (m_4\boldsymbol{g_b}) + \boldsymbol{\rho_{w_4,b}} \times (m_5\boldsymbol{g_b}) \end{aligned} \tag{19}$$

$$\begin{bmatrix} Q_4 \\ Q_5 \\ Q_6 \end{bmatrix} = \begin{bmatrix} L \\ M \\ N \end{bmatrix} + \boldsymbol{M_g} \begin{bmatrix} \boldsymbol{b}_x \\ \boldsymbol{b}_y \\ \boldsymbol{b}_z \end{bmatrix} \tag{20}$$

The last generalized force, Q_7, is the moment applied by the motor (M_m) to flap the wings, defined as:

$$Q_7 = M_m \tag{21}$$

7) D'Alembert's Method For Rigid Bodies: All the previous derivations can now be used to calculate the aerodynamic forces and moments acting on the FWMAV using d'Alembert's dynamic principle of virtual work, which is expressed as:

$$\sum_{i=1}^{N} [m_i(\dot{\boldsymbol{v}}_{\boldsymbol{i}} + \ddot{\boldsymbol{\rho}}_{ci})\boldsymbol{\gamma_{ij}} + (I_i\dot{\boldsymbol{\omega}}_i + \boldsymbol{\omega}_i \times I_i\boldsymbol{\omega}_i + m_i\boldsymbol{\rho}_{ci} \times \dot{v}_i)\boldsymbol{\beta_{ij}}] = Q_j \tag{22}$$

In this equation, i is the body index and j is the quasi-velocity or generalized force index. The velocity coefficient matrix $\boldsymbol{\gamma}_{ij}$ and the angular velocity coefficient $\boldsymbol{\beta}_{ij}$ are calculated by differentiating the linear and angular velocities of each body with respect to each the quasi-velocities, using:

$$\boldsymbol{\gamma}_{ij} = \frac{\partial \boldsymbol{v}_i}{\partial \boldsymbol{u}_j} \tag{23}$$

$$\boldsymbol{\beta}_{ij} = \frac{\partial \boldsymbol{\omega}_i}{\partial \boldsymbol{u}_j} \tag{24}$$

These 7 equations of motion are completed by 7 other formulas that relate $\dot{q}_j$ with $\boldsymbol{u}_j$, Eqs. 25 and 26:

$$\begin{bmatrix} \dot{x} \\ \dot{y} \\ \dot{z} \end{bmatrix} = \mathcal{R}_{E,b} \begin{bmatrix} u \\ v \\ w \end{bmatrix} \tag{25}$$

$$\begin{bmatrix} \dot{e_0} \\ \dot{e_1} \\ \dot{e_2} \\ \dot{e_3} \end{bmatrix} = 2 \begin{bmatrix} 0 & -p & -q & -r \\ p & 0 & r & -q \\ q & -r & 0 & p \\ r & q & -p & 0 \end{bmatrix} \begin{bmatrix} e_0 \\ e_1 \\ e_2 \\ e_3 \end{bmatrix} \tag{26}$$

IV. Results and Discussion

The forces and moments were found to have very similar relative evolutions throughout the several flights. Hence, for objectiveness and ease of comprehension, the results are presented for trimmed flight and two system identification maneuvers: doublet input on the rudder and doublet input on the elevator, with the input duration of $\frac{2}{3}$ seconds ($\frac{1}{3}$ second to each side).

A. Results

The results follow the same structure as the previous sections: first the FWMAV's position and reconstructed states are presented, for a maneuver with a doublet input on the rudder, in Figures 7 to 13; second, the calculated forces and moments are presented for both kinematic formulations in Figures 14 and 15.

The aerodynamic forces and moments of 4 seconds of flight were computed for the elevator input maneuver and are presented in Figures 16 and 17. The states for this maneuver can be found in [8].

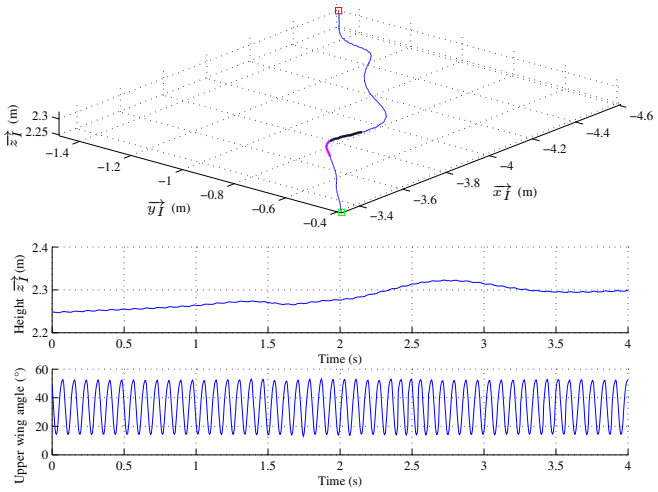

Fig. 7. Directly measured states, from the external visual tracking system, after filtering: (top) the FWMAV's CG position in the Inertial reference frame - the green and red markers indicate the initial and final position respectively, whereas the magenta and black lines indicate the rudder deflection to the right and to the left respectively; (middle) the height during flight; (bottom) the upper wing angle, with respect to the body frame.

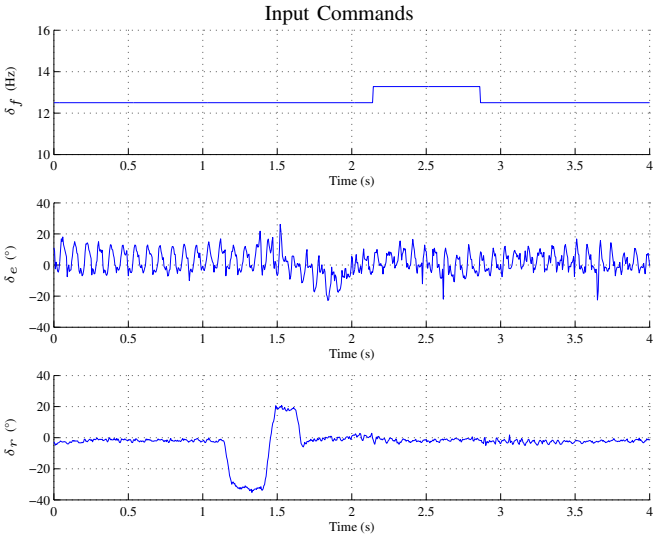

Fig. 8. Control surface states: (top) flapping frequency δ_f in Hz; (middle) elevator angle deflection δ_e in (°) where positive is elevator down; (bottom) rudder angle deflection δ_r in (°), where positive is rudder to the left. A doublet input of $\frac{2}{3}$ seconds to the rudder was commanded at 1.15 seconds .

B. Discussion

There is a dominant oscillatory motion in all states, as well as in the elevator and rudder positions that are induced by the flapping motion described in Figure 7 (bottom plot).

The square nature of the flapping frequency (δ_f) observed in Figure 8 (top) is due to the limited resolution on the wing angle over a flap cycle. The values correspond to $\frac{200}{15}$Hz and $\frac{200}{16}$Hz, with the denominator being the number of samples per flap cycle.

The rudder deflection input (Figure 8) affects all attitude angles, i.e., the first deflection to the right, induced a roll ϕ_r angle of 50°, a yaw rotation ψ_y of 70° and a pitch (θ_p) variation of 10° downwards; the second deflection, to the left, induced an opposite rotation in all axis, compensating for the first attitude variation. It, however, also aggravated the pitch variation due to the high vertical placement of the rudder with respect to the DelFly's CG, that in this case was of 30mm.

The wing stroke plane angle, that is almost parallel to $\overrightarrow{z_b}$, and the consequent inertia changes around $\overrightarrow{x_b}$ affect mostly the longitudinal states. In particular, the wing flap affects the pitch angle θ_p (Figure 9) that, in turn, will affect the

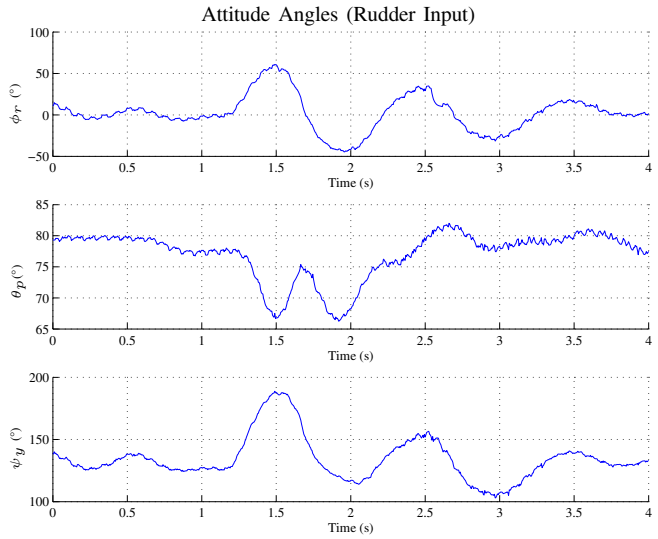

Fig. 9. Attitude angles along the Body axis, reconstructed from corresponding Direct Cosine Matrix into a 3-2-1 Euler angle rotation matrix:(top) roll ϕ_r;(middle) pitch θ_p ;(bottom) yaw ψ_y [8].

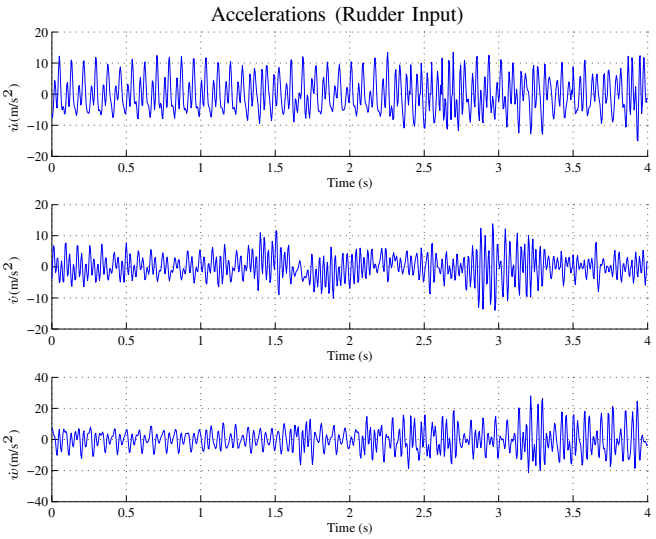

Fig. 11. Acceleration components of the ornithopter's CG along its Body axis. $\dot{u}$ and $\dot{w}$ were mostly affected by flapping motion, whereas $\dot{v}$ has a coupled effect from the rudder input maneuver and the flapping motion.

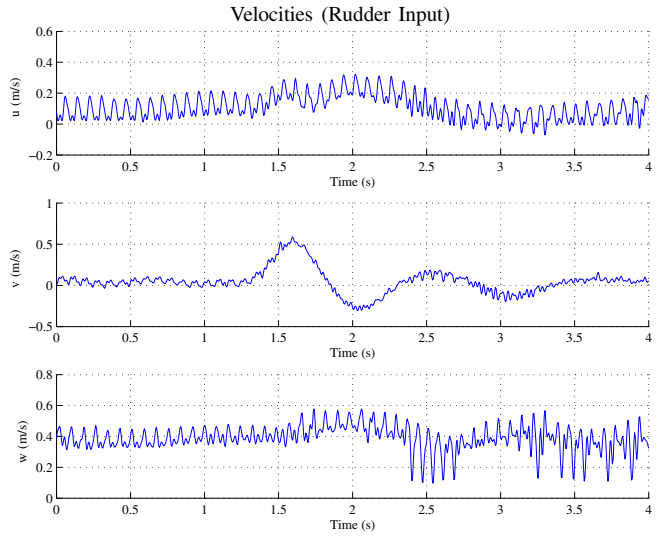

Fig. 10. Velocity components of the ornithopter's CG along its Body axis. The velocities along $\overrightarrow{x_b}$ and $\overrightarrow{z_b}$ (u and w) are mostly affected by the flapping motion, whereas v is very affected by the lateral motion, induced by the commanded deflection of the rudder.

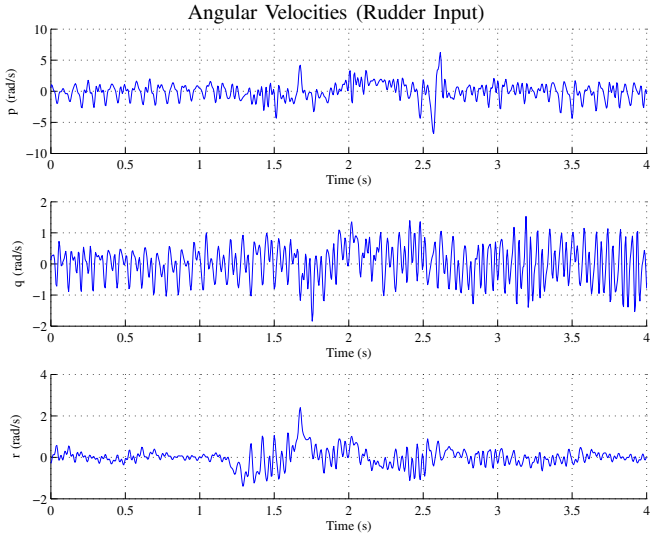

Fig. 12. Angular velocities of the DelFly around its Body axis. Highly affected by the flapping motion as well as by the input on the rudder, performed at 1.15 seconds.

velocity and acceleration along $\overrightarrow{x_b}$ and $\overrightarrow{z_b}$ (Figures 10 and 11, respectively), as well as pitch rate p and the pitch acceleration $\dot{p}$ (Figures 12 and 13).

The linear and angular velocities, in Figures 10 and 12 respectively, were also affected by the input. In particular, the lateral velocity v and angular velocities p and r had the biggest oscillations. After the rudder input, the platform returned to its initial flight regime, by dampening the long period oscillations.

The linear and angular accelerations used in the kinematic models are presented in Figures 11 and 13, respectively. Comparing these with the respective velocities, one can see that the fast sub-flap oscillations are dominant over the maneuver induced oscillations.

Despite these flap induced oscillations, the aerodynamic forces' evolution presented in Figures 14 and 16 shows that both kinematic derivations lead to very similar aerodynamic forces and moments, even in highly non-linear maneuvers caused by the doublet on the rudder.

Among the forces, the Z force of the elevator maneuver (Figure 16) had the biggest differences between both methods, while X reveals an almost perfect match. The differences in Z are caused by the wings' deceleration at the end of the out-stroke, where the flap angle is maximum, which has a bigger influence due to the fact that the wings' stroke plane

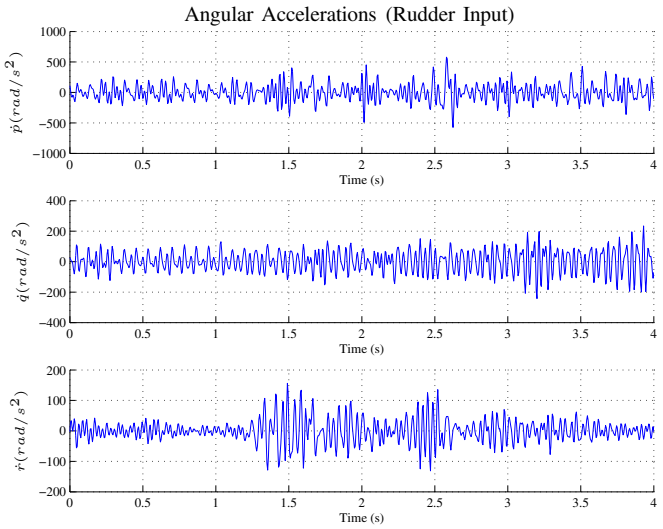

Fig. 13. The ornithopter's angular accelerations around its Body axis. These were mainly affected by the flapping motion which induced rapid change the angular body rates p, q and r. $\dot{r}$ was the most affected angular acceleration by the maneuver input which is justified by the direct effect of the rudder deflection.

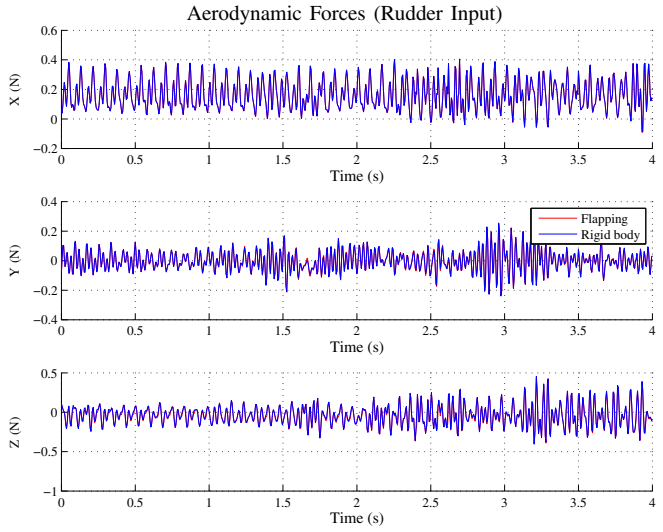

Fig. 14. Aerodynamic forces using rigid body Newton-Euler equations of motion (blue) and d'Alembert's equations for 5 coupled rigid bodies (red). Both formulations resulted in similar evolutions, with *X* being the least affect force; *Y* had very close results as well, which sustains the symmetry assumption made in the rigid body formulation; the different *Z* evolutions were due to the inertia and mass effect of the wing motion in the stroke plane, that is almost parallel to the $\overrightarrow{z_b}$.

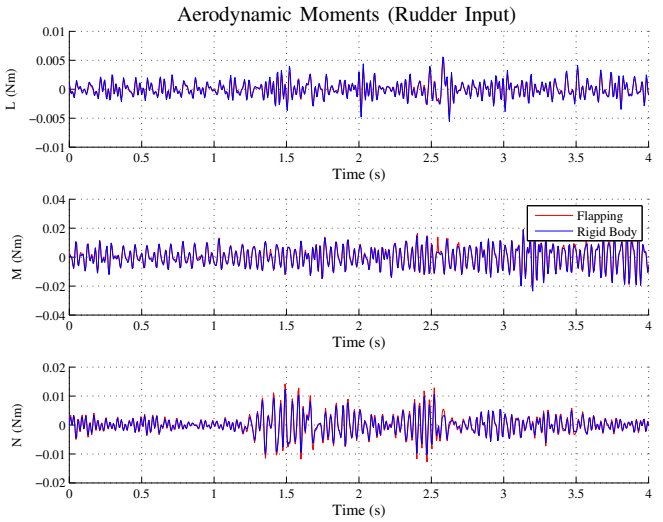

Fig. 15. Aerodynamic moments that were calculated using rigid body Newton-Euler equations of motion (blue) and d'Alembert's equations for 5 coupled rigid bodies (red). The *N* moments differ between both methods mainly due to the effect of the mass and inertia of the wings in the yaw rate states r and $\dot{r}$; this effect is not much notorious in *L* and *M*.

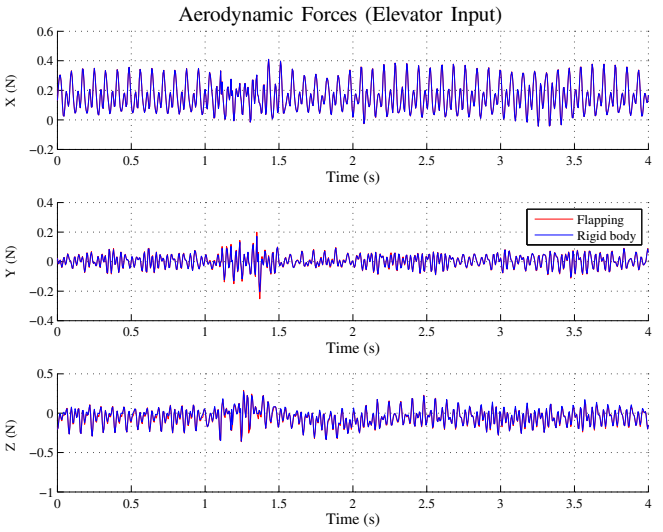

Fig. 16. Aerodynamic forces using rigid body Newton-Euler equations of motion (blue) and d'Alembert's equations for 5 coupled rigid bodies (red). The forces present an evolution that is similar to the rudder input maneuver, with *Z* presenting the biggest differences, due to the inertia and mass effects of the flapping wings and the maneuver induced by the elevator input.

is almost parallel to the $\overrightarrow{z_b}$ axis. This results in added pitch inducing forces along $\overrightarrow{z_b}$ which, in turn, induce variations in the pitch moment between both methods, as indicated in Figures 15 and 17.

The higher amplitude of the flapping wing kinematics *N* moment (Figures 15 and 17) is caused by the added inertia effect of the wings, i.e., the contribution of the 4 wings' moments of inertia (Table III) around $\overrightarrow{z_b}$, as a bigger *N* moment is needed to accelerate more inertia with the same angular acceleration.

Pearson's Correlation Coefficient (PCC) was used to quantify the similarities between both kinematic methods. This method establishes a liner correlation between two signals evaluating the way they vary with respect to their mean and is defined as the covariance (cov) of 2 signals divided by the product of the standard deviation (σ) of each signal (Eq. 27). Two totally correlated, uncorrelated and negative-correlated signals have a PCC of 1, 0 and -1 respectively.

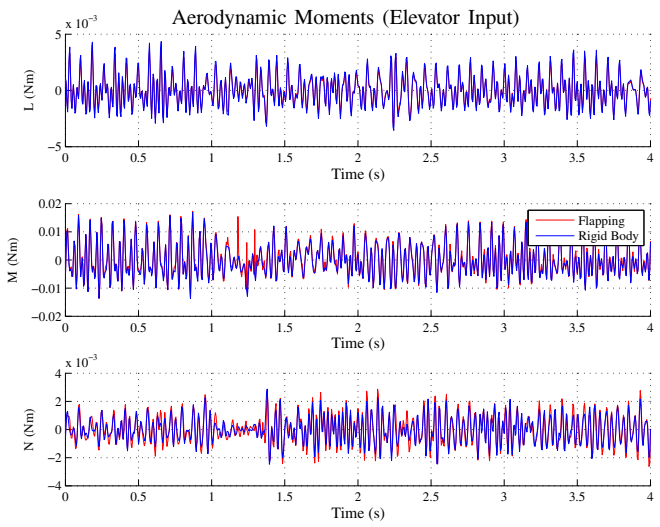

Fig. 17. Aerodynamic moments using rigid body Newton-Euler equations of motion (blue) and d'Alembert's equations for 5 coupled rigid bodies (red). These moments present a similar evolution to the rudder input, with the *N* moments differing the most between methods, due to the mass and inertia effects of the wings, not considered in the rigid body equations; the *M* moment is more affected during the maneuver due to the added mass and inertia effect of the wings in the vertical pitch plane $x_b z_b$.

$$pcc_{F_{rb},F_{flap}} = \frac{\text{cov}(F_{rb}, F_{flap})}{\sigma(F_{rb})\sigma(F_{flap})} \tag{27}$$

TABLE IV
PEARSON'S CORRELATION COEFFICIENT RESULTS FOR BOTH MANEUVERS. THE FORCES AND MOMENTS EVIDENCED A VERY CLOSE FORM AND PHASE, WITH CORRELATIONS ALWAYS ABOVE 0.95.

Forces and Moments	X	Y	Z	L	M	N
Doublet Rudder	0.99	0.99	0.98	0.98	0.99	0.98
Doublet Elevator	0.99	0.99	0.97	0.99	0.97	0.95

The correlation coefficients were found to the be very high, close to 1, for all forces and moments, as indicated in Table IV, indicating a big linear correlation between the calculated forces and moments.

This study has revealed that simple equations of motion are still applicable to force and moment reconstruction of free flying FWMAVs, for cases where the rocking oscillations are small, in the particular case of ornithopters with 4 wings and also 2 winged ones whose wings' mass or area are small when compared to the rest of the body. Moreover, these equations should still be able to predict the forces and moments of bird and bat inspired ornithopters, in which the pitch oscillations are dampened by the presence of a tail.

Despite being more complex, detailed multi-body kinematics like the ones described here allow the direct assessment of control forces and moments over the individual wings and motors, which has clear benefits over rigid body formulations. In the present case, a 7^{th} generalized force Q_7 could be calculated, which describes the flapping motor torque. These formulations gain over rigid body equations for FWMAVs that depend on active control of more than 1 DOF of the wings, in the case of insect inspired tailless designs.

Moreover, the use of Quaternions on the flapping formulation has beneficial effects in computational efficiency, as well as in avoiding singularity issues of the Euler angles.

V. CONCLUDING REMARKS

Flapping wing aerial vehicles are complex dynamic systems. Consequently, their descriptive equations of motion are very often difficult to derive. Hence, system identification techniques and dynamic simulation of these systems would benefit from having simpler, but still physically representative kinematic derivations that could be used to capture or simulate the aerodynamic forces and moments in free flight.

This study quantitatively compared the aerodynamic forces and moments that were computed from free flight data using two kinematic formulations devised under different assumptions: 1) rigid body equations of motion, using Newton-Euler formulation, commonly know as the general aircraft equations of motion and 2) multi-body flapping wing kinematics using d'Alembert's principle.

The results showed the applicability of rigid body kinematics for determining the aerodynamic forces and moments acting on the FWMAV, showing a very high proximity to the correspondent forces and moments calculated using much more complex flapping wing kinematics.

The forces along the longitudinal and lateral Body axes $\overrightarrow{x_b}$ and $\overrightarrow{y_b}$, *X* and *Y* respectively, matched almost perfectly between both methods. The differences in the *Z* force, which acts in the direction of the Body axis $\overrightarrow{z_b}$, can be explained by lack of wing symmetry around the $x_b y_b$ plane, which introduced an added inertia effect caused by the upper wings' deceleration at the end of the out-stroke. In particular, the wing dihedral, the rotation hinge around $\overrightarrow{x_b}$ and stroke plane angle which is almost parallel to $\overrightarrow{z_b}$ induced added mass effects on the *Z* force which, in turn, also contributed to the small differences evidenced in the moment *M* around $\overrightarrow{y_b}$.

The differences in the *L* and *N* moments are caused by the added inertia effects of wings for body rotations around $\overrightarrow{x_b}$ and $\overrightarrow{z_b}$, accounted for in the flapping kinematics.

A linear correlation was established between the results of both methods, with correlation factors higher than 0.95 for all external forces and moments.

More descriptive formulations that use multi-body kinematics do have advantages for complex FWMAVs, especially the ones with more than 1 DOF on the wings, as well as for tailless designs. In that case, multi-body kinematic formulations allow control force and moment determination, which is required for active control and dynamic simulation.

Nevertheless, the results indicate that simple rigid body aircraft equations of motion are still applicable to FWMAV system identification and control design, allowing a faster assessment and comparison between different FWMAV designs, as well as allowing for faster implementation of non-linear dynamic simulations.

REFERENCES

[1] M. Keennon, K. Klingebiel, and H. Won, "Development of the nano hummingbird: A tailless flapping wing micro air vehicle," in *50TH AIAA AEROSPACE SCIENCES MEETING INCLUDING THE NEW HORIZONS FORUM AND AEROSPACE EXPOSITION*, pp. 1–24, 2012.

[2] R. Wood, "The first takeoff of a biologically-inspired at-scale robotic insect," *IEEE Tranactions on Robotics*, vol. 24(2), pp. 341–347, 2008.

[3] P. Chirarattananon, K. Y. Ma, and R. J. Wood, "Adaptive control for takeoff, hovering, and landing of a robotic fly," in *Proceedings IEEE/RSJ International Conference on Intelligent Robots and Systems*, (Tokyo, Japan), pp. 3808–3815, November 2013.

[4] L. L. Hines, V. Arabagi, and M. Sitti, "Free flight simulations and pitch and roll control experiments of a sub-gram flapping-flight micro aerial vehicle," in *Proceedings - IEEE International Conference on Robotics and Automation*, (Shanghai, China), IEEE, May 2011.

[5] S. Baek and R. Fearing, "Flight forces and altitude regulation of 12 gram i-bird," in *IEEE RAS and EMBS International Conference on Biomedical Robotics and Biomechatronics (BioRob)*, pp. 454–460, 2010.

[6] Delfly Team, "Delfly." www.delfly.nl, accessed on January 5th, 2014.

[7] G. de Croon, K. de Clercq, R. Ruijsink, B. Remes, and C. de Wagter, "Design, aerodynamics, and vision-based control of the DelFly," *International Journal of Micro Air Vehicles*, vol. 1, no. 2, pp. 71–97, 2009.

[8] J. V. Caetano, C. de Visser, G. de Croon, B. Remes, C. de Wagter, J. Verboom, and M. Mulder, "Linear aerodynamic model identification of a flappingwing mav based on flight test data," *International Journal of Micro Air Vehicles*, vol. 5, pp. 273–286, December 2013.

[9] S. S. Baek, F. L. G. Bermudez, and R. S. Fearing, "Flight control for target seeking by 13 gram ornithopter," in *IEEE Int. Conf. Intelligent Robots and Systems*, September 2011.

[10] S. Tijmons, G. de Croon, B. Remes, C. de Wagter, R. Ruijsink, E.-J. van Kampen, and Q. P. Chu, "Stereo Vision based Obstacle Avoidance on Flapping Wing MAV," in *Euro Guidance, Navigation an Control Conference, EGNC 2013*, (Netherlands), EGNC, 2013.

[11] G. Gebert and P. Gallmeier, "Equations of motion for flapping flight," in *AIAA Atmospheric Flight Mechanics Conference and Exhibit*, no. 2002-4872, August 2002. AIAA.

[12] J. Grauer, E. Ulrich, J. H. Jr., D. Pines, , and J. S. Humbert, "Testing and system identification of an ornithopter in longitudinal flight," *Journal of Aircraft*, vol. 48, pp. 660–667, March-April 2011.

[13] J. Grauer, E. Ulrich, J. H. Jr., D. Pines, and J. S. Humbert, "System identification of an ornithopteraerodynamics model," No. 2010-7632, AIAA, August 2010.

[14] C. T. Orlowski, A. R. Girard, and W. Shyy, "Four wing flapping micro air vehicles - dragonfies or x-wings?," in *AIAA Guidance, Navigation, and Control Conference* (AIAA, ed.), (Toronto, Ontario, Canada), AIAA, August 2010.

[15] C. T. Orlowski and A. R. Girard, "Modeling and simulation of nonlinear dynamics of flapping wing micro air vehicles," *AIAA Journal*, vol. 49, pp. 969–981, May 2011.

[16] M. A. Bolender, "Rigid multi-body equations-of-motion for flapping wing MAVs using Kane equations," in *AIAA Guidance, Navigation, and Control Conference*, no. 2009-6158, AIAA, August 2009.

[17] W. Su and C. E. S. Cesnik, "Nonlinear aeroelastic simulations of a flapping wing micro air vehicle using two unsteady aerodynamic formulations," vol. 2010-2887, (Orlando, Florida), University of Michigan, AIAA, April 2010.

[18] W. Su and C. E. S. Cesnik, "Flight dynamic stability of a flapping wing micro air vehicle in hover," vol. 2011-2009, (Denver), University of Michigan, AIAA, April 2011.

[19] J. M. Dietl and E. Garcia, "Stability in ornithopter longitudinal flight dynamics," *Journal of Guidance, Control and Dynamics*, vol. 31, pp. 1157–1162, 2008.

[20] J. M. Dietl, T. Herrmann, G. Reich, and E. Garcia, "Dynamic modeling, testing, and stability analysis of an ornithoptic blimp," *Journal of Bionic Engineering*, vol. 8, no. 8, pp. 375–386, 2011.

[21] J. V. Caetano, C. C. de Visser, B. Remes, C. de Wagter, and M. Mulder, "Controlled flight maneuvers of a flapping wing micro air vehicle: a step towards the DelFly II identification," in *AIAA Atmospheric Flight Mechanics Conference*, 2013.

[22] J. V. Caetano, C. C. de Visser, B. Remes, C. de Wagter, and M. Mulder, "Modeling a Flapping Wing MAV: Flight Path Reconstruction of the DelFly II," in *AIAA Modeling and Simulation Technologies*, AIAA, 2013.

[23] B. L. Stevens and F. L. Lewis, *Aircraft Control and Simulation*. Jonh Wiley & Sons, Inc., 2 ed., 2003.

[24] W. F. Phillips, C. E. Hailey, and G. a. Gebert, "Review of Attitude Representations Used for Aircraft Kinematics," *Journal of Aircraft*, vol. 38, pp. 718–737, July 2001.

[25] H. Baruh, *Analytical Dynamics*. McGraw-Hill Higher Education, 1999.